Research Square

Preprints are preliminary reports that have not undergone peer review.
They should not be considered conclusive, used to inform clinical practice,
or referenced by the media as validated information.

Immune Control of Oncogene Selection in the Colon.

Haris Mirza

haris.mirza@yale.edu

Department of Pathology, Yale School of Medicine; Department of Immunobiology, Yale School of Medicine

Birgit Tschiatschek*

Institute of Biology, University of Graz

Miraal Maqsood*

Department of Pathology, Yale School of Medicine

Xumin Li

Department of Epidemiology, University of Washington

Min-Hee Oh

Department of Immunobiology, Yale School of Medicine

Esen Sefik

Department of Immunobiology, Yale School of Medicine

Fengrui Zhang

Department of Immunobiology, Yale School of Medicine

Shun-Fat Lau

Department of Immunobiology, Yale School of Medicine https://orcid.org/0000-0002-8527-3205

Shahistha Hashim

Department of Pathology, Yale School of Medicine

Viktoria Juric

Department of Pathology, Yale School of Medicine

Frank Tran

Department of Immunobiology, Yale School of Medicine

Kriti Agrawal

Department of Pathology, Yale School of Medicine; Department of Immunobiology, Yale School of Medicine https://orcid.org/0000-0002-5778-6118

Nicole Blackburn

Department of Immunobiology, Yale School of Medicine

Manolis Roulis

Department of Pathology and Laboratory Medicine, University of Pennsylvania

Oluwabunmi Olaloye

Department of Pediatrics, Yale School of Medicine

Liza Konnikova

Department of Immunobiology, Yale School of Medicine; Department of Pediatrics, Yale School of Medicine; Department of Obstetrics, Gynecology and Reproductive Sciences https://orcid.org/0000-0003-4804-5497

Gundolf Haase

Department of Mathematics and Scientific Computing, University of Graz

Yuval Kluger

Department of Pathology, Yale School of Medicine; Department of Immunobiology, Yale School of Medicine https://orcid.org/0000-0002-3035-071X

Benjamin Simons

Gurdon Institute, University of Cambridge https://orcid.org/0000-0002-3875-7071

Bernat Corominas-Murtra

bernat.corominas-murtra@uni-graz.at

Institute of Biology, University of Graz https://orcid.org/0000-0001-9806-5643

Richard Flavell

richard.flavell@yale.edu

Department of Immunobiology, Yale School of Medicine https://orcid.org/0000-0003-4461-0778

Biological Sciences - Article

Keywords:

Posted Date: February 26th, 2026

DOI: https://doi.org/10.21203/rs.3.rs-8673399/v1

License: This work is licensed under a Creative Commons Attribution 4.0 International License. Read Full License

Additional Declarations:
Yes there is potential Competing Interest. RAF is a consultant in Geneta Science and Evolveimmune Therapeutics Inc.

All animal experimentation on non-human vertebrates in this study was approved and performed under the oversight, and in compliance with Yale Institutional Animal Care and Use Committee (IACUC) protocols.

Immune Control of Oncogene Selection in the Colon.

Haris Mirza[1,2,#], Birgit Tschiatschek[3,*], Miraal Maqsood[1,*], Xumin Li[4], Minhee Oh[2], Esen Sefik[2], Fengrui Zhang[2], Shun-Fat Lau[2], Shahistha Hashim[1], Viktoria Juric[1], Frank Tran[2], Kriti Agrawal[1,2], Nicole Blackburn[2], Manolis Roulis[5], Oluwabunmi Olaloye[6], Liza Konnikova[2,6,7], Gundolf Haase[8], Yuval Kluger[1,2], Benjamin Simons[9], Bernat Corominas-Murtra[3,#], Richard Flavell[2,#]

[1]Department of Pathology, Yale School of Medicine
[2]Department of Immunobiology, Yale School of Medicine
[3]Institute of Biology, University of Graz
[4]Department of Epidemiology, University of Washington
[5]Department of Pathology and Laboratory Medicine, University of Pennsylvania
[6]Department of Pediatrics, Yale School of Medicine
[7]Deaprtment of Obstetrics, Gynecology and Reproductive Sciences
[8] Department of Mathematics and Scientific Computing, University of Graz
[9]Gurdon Institute, University of Cambridge

Corresponding authors: richard.flavell@yale.edu; bernat.corominas-murtara@uni-graz.at ; haris.mirza@yale.edu
* Contributed equally

Abstract

Crypt fixation is an early and essential event of colorectal cancer initiation [1–6]. It is an evolutionary process where precancerous stem cells compete with their healthy neighbors for monoclonal fixation of intestinal crypts [1–6]. This competition involves stochastic interaction between three cell populations, oncogene mutant clones, competing wild-type clones and the cells populating their microenvironment. Interactions between competing WT and mutant clones are well studied; however, the impact of the microenvironment cells on crypt fixation, has been challenging to quantify [1–6]. This is due to the absence of suitable experimental and theoretical models to study three-way stochastic interactions between competing clones and cells in their microenvironment. To overcome this challenge, we integrated established mosaic clonal selection models[1,7,8] and immune depletion models[9] with the theoretical framework provided by Stochastic

Conveyor Belt model [10,11]. Using this approach, we quantified the selective advantage of colonic stem cells with the *BRAF*^{V600E} mutation, one of the most prevalent human oncogenes. We showed that *BRAF*^{V600E} confers a selective advantage to colonic stem cells but approximately half of the clones are destined for clonal extinction. We show mechanistically that clonal extinction of these precancerous cells is actively mediated by adaptive immune system. Specific depletion of regulatory T cells or targeted deletion of Major Histocompatibility Complex Class II *(MHCII*) or interleukin 10 receptor A (*IL10RA*) on the *BRAF*^{V600E} mutated clones, prevented their extinction. Overall, these findings reveal a new immune sensing mechanism whereby Tregs recognize and eliminate precancerous stem cells before malignant transformation. Understanding this interplay between microenvironment and stem cell dynamics at tumor initiation will enable the development of immunoprevention strategies against colon cancer initiation, rather than treat existing tumors.

Main

Fixation of intestinal crypts by an oncogenic mutation is one of the earliest and essential events of tumor initiation [1–6]. It is an evolutionary process where stem cell clones compete for supremacy [1–6]. The 'Winner' clone forces the extinction of the competing clones and populates the entire crypt with its progeny [1–6]. Oncogenic mutations confer a selective advantage to the mutated stem cells, increasing their probability of clonal fixation by biased drift [1–6]. Once fixed, the oncogenic clones are at high risk of malignant transformation [8,12–14] due to their persistence, rapid expansion[2,15–17] and accelerated mutagenesis [8,12–14,18]. Fortunately, despite their selective advantage, the majority of oncogenic clones do not reach the crucial threshold of crypt fixation and are destined for

clonal extinction[1,2]. This makes clonal extinction one of the most effective tumor-suppressing mechanism in the colon.

Clonal fixation of an oncogenic mutation is determined by complex interactions between three cell populations, wild type (WT) stem cells, a newly emergent oncogenic clone and the microenvironment cells[1,2,5,12,14,19–21]. While there are several studies highlighting elimination of WT cells by oncogene mutated clones. and vice versa [1,2,4,6,12,14–16], how the microenvironment cells impact crypt fixation of oncogenes is unknown. This is due to the absence of suitable experimental and theoretical models to study three-way stochastic interactions between competing clones and their microenvironment.

Intestinal stem cell microenvironment comprises of diverse cell types, including paneth cells[22], fibroblasts[23,24], endothelial cells[25] as well as a crucial and abundant population of immune cells[26,27]. The role of immune cells in the colon cancer pathogenesis and treatment is undeniable[28–30]. However, whether immune system surveils precancerous tissues against oncogenes is not known. To investigate this potential oncogene surveillance function, we chose the V600E mutation in the MAP kinase pathway gene BRAF. This mutation is one of the most prevalent human oncogenes[31], attributed to its purported proficiency in evading immune surveillance[28]. Paradoxically, $BRAF^{V600E}$ is also highly immunogenic[32]. In the colon, it is sufficient to initiate the “serrated pathway” of tumorigenesis which is marked by a heavy infiltration of lymphocytes in the tumor microenvironment[33]. These characteristics make the *$BRAF^{V600E}$* mutation an ideal candidate for investigating the role of the immune system in oncogene selection.

Whether *BRAF*^{V600E} mutation actually endows colonic stem cells with a selective advantage is not known. Thus, in this study, using precise lineage tracing mouse models, single cell RNAseq, combined with the quantitative predictions provided by the *Stochastic Conveyor Belt* (SCB) theoretical framework[11,34,35], we investigated the selective advantage of *BRAF*^{V600E} mutation in the colon. More importantly we identified that immune cells sense the presence of *BRAF*^{V600E} clones and promote their extinction from the colon.

Extinction of *BRAF*^{V600E} clones from the colon.

To investigate the impact of the *BRAF*^{V600E} mutation in the colonic epithelium, we performed single cell RNA seq at an early point (day 6) following oncogene induction, using VilinCre^{ERT2} system (fig. 1a-c). Overall, *BRAF*^{V600E} expression expands undifferentiated stem and progenitor cell populations (fig. 1c and d, Extended fig. 1a and b) and impairs their differentiation into both secretory and enterocyte lineages. In addition to aberrant differentiation, mutated colonic stem cells also show a significant increase in proliferation (fig. 1e and f, Extended fib. 1c), with significant upregulation of *mki67, Mcm6*, *Top2A* and *Ccnd1* gene expression.

Pro-proliferative, KRAS and APC mutations confer a selective advantage to intestinal stem cells[1,2]. To investigate whether the highly proliferative BRAF^{V600E} mutated stem cells possess a comparable selective advantage over their WT neighbors, we induced the *BRAF*^{V600E} mutation via an established low-level mosaic recombination method using the *Villin-Cre*^{ERT2} mouse strain, coupled with a low-dose of tamoxifen[8,15] (fig. 1h). Clones were visualized and quantified at the bottom of the colonic crypts using a lineage tracing confetti reporter allele to ensure observation of monoclonal expansion

from a single mutant stem cell (fig. 1i). The average clone size and number of monoclonal fixed clones increased in the colon over time in *BRAF*^{V600E} mutated cells at a significantly higher rate compared to WT cells (fig 1j and k), suggesting a positive selection of *BRAF*^{V600E} clones.

To resolve and quantify the selection dynamics of *BRAF*^{V600E} mutant clones, we assumed the dynamical hypothesis of the stem cell competition of the *Stochastic Conveyor Belt* framework (SCB) (fig.1 g, supplementary theory) [11,34,35]. The dynamical hypothesis of the SCB model considers that cells undergo two core processes 1) cell division at rate k_d (with random division orientation), leading to the upward transfer of cells along the crypt axis and 2) random cell relocation at constant rate k_r, directed upward or retrograde movement towards the crypt base (fig 1g, supplementary theory). By application of the SCB model to our 'neutral' WT clonal data, a relocation rate of k_r=0.0525 and proliferation rate k_d= 0.21 per day was calculated. Accordingly, the ratio k_r/k_d = 0.25 ratio (fig. 1j) is maintained in full agreement with the previously published results for the k_r/k_d ratio in the colon[10]. Thus far, the SCB model has only been used to study 'neutral' competition between WT cells in a crypt[10]. To model 'biased' competition between the WT and oncogene (*BRAF*^{V600E}) mutated cells, we used the following parameters: relocation rate k_r=0.0525 was kept constant for all cell populations (WT and mutant) and proliferation rate k_d=0.21 was kept for all WT clones. Additionally, a single mutant clone was assigned an altered proliferation rate k_d^{μ}. With this modelling setup, we predicted, an increased division rate, reaching k_d^{μ} =0.46 for the mutant clones, almost twice of that of WT clones (fig. 1j). These calculations are consistent with the increased proliferation index of *BRAF*^{V600E} stem cells in our single cell analysis (figure 1e and f) and a higher proliferation

rate of *BRAF*^{V600E} mutated colonic cells reported previously[36,37]. The higher mutant proliferation rate k_d^{μ} was also sufficient to account for the significantly increased crypt fixation rate of *BRAF*^{V600E} clones observed in our in-vivo studies (fig. 1j). Using the above parameters for relocation (k_r), WT cell division (k_d) and mutant (BRAF^{V600E}) cell division (k_d^{μ}) rates, the SCB model predicted that a *BRAF*^{V600E} cell replaces its WT neighbor with the probability of ~0.7, thereby confirming biased selection of *BRAF*^{V600E} mutant clones (fig. 1k). It is worth mentioning that, by definition, in the neutral scenario, a WT cell replaces its WT neighbor cell with probability 0.5 and vice versa[1,10,38,39]. The outcome of this selective advantage is the significantly higher probability of the *BRAF*^{V600E} mutated stem cells to fix the colonic crypt (0.48±0.05) via biased drift, compared to fixation probability of WT clones via neutral drift (0.115±0.03) (fig,1l, extended fig. 1d and e). Interestingly, despite having an obvious selective advantage, the majority of the *BRAF*^{V600E} mutant stem cells in the colon, fail to reach crypt fixation (fig, 1l, extended fig, 1d and e) and are destined for extinction (0.522 ± 0.049) (fig, 1l, extended fig, 1d and e).

MHCII dependent extinction of BRAF^{V600E} clones.

To investigate the mechanisms of crypt fixation, we compared the gene expression signatures of colonic stem cells following induction of *BRAF*^{V600E} mutation (fig. 2a-e). We noted an enrichment of immune response related pathways in the *BRAF*^{V600E} mutated stem cells (fig. 2d) particularly, major histocompatibility class II (MHCII) related genes *H2-Ab1*, *H2-DMb1*, *H2-Aa*, *H2-Eb1* and *CD74* (fig. 2d). MHCII proteins are a critical component of professional antigen presentation cells (Macrophages/ monocytes, dendritic cells and B-cells). They are not expressed in healthy colonic stem cells[40]. In the small intestine however, they assist in eradication of infection[26]. Expression of MHCII in

147 *BRAF*^{V600E} mutated cells is accompanied by upregulation of *CIITA*, trans activator of
148 MHCII pathway as well as a concomitant activation of interferon gamma pathway genes
149 (*B2m*, *Irf9* and *Irf1*), classical components of MHCII pathway activation in APCs (fig. 2e,
150 extended fig. a and b).

151 Fitness sensing is a highly conserved mechanism through which tissues identify
152 winners and losers of cell-cell competition, thereby applying an evolutionary pressure
153 against selection of undesirable, loser cells[41]. In human tissues, MHCII has been
154 predicted to exerts an evolutionary pressure against selection of oncogenic mutations via
155 poorly understood mechanisms[32]. To investigate if MHCII expression in BRAF^{V600E}
156 mutated colonic stem cells performs a fitness sensing function, we crossed our lineage
157 tracing mice with *MHCII*$^{fl/fl}$ mice to generate a model that specifically deletes all
158 components of MHCII from *BRAF*^{V600E} mutated cells, leaving MHCII expression intact in
159 the rest of the system (fig 2f). MHCII deletion (*MHCII*$^{fl/fl}$) in BRAFV600E clones,
160 significantly increased the rate of clonal fixation compared to monoallelic (*MHCII*$^{fl/+}$)
161 controls (fig 2g and h).

162 Keeping the relocation rate constant at k_r = 0.0525 and the WT division rate at k_d
163 = 0.21 in our SCB model, the proliferation rate for *BRAF*^{V600E}*; MHCII*$^{fl/fl}$ mutant clones
164 was calculated to be k_d^{μ} = 0.74 which was significantly higher than *BRAF*^{V600E} clones with
165 intact MHCII expression (*BRAF*^{V600E}*; MHCII*$^{fl/+}$*;* k_d^{μ} = 0.45) (fig. 2h). With these
166 parameters, the probability of *BRAF*^{V600E}; mutant clones replacing its WT neighbor was
167 increased to ~0.81, following MHCII deletion (fig. i). The outcome of this increased
168 selective advantage is that loss of MHCII in a *BRAF*^{V600E} clone, decreases its probability
169 of extinction from the colonic crypts (0.343 ± 0.047) (fig. 2j, extended fig. 4a). These

findings are consistent with higher prevalence of *BRAF*^{V600E} mutated tumors in patients with impaired MHCII antigen presentation[32]. This is also the first evidence that MHCII expression on stem cells serves as a potent tumor suppressive mechanism, by promoting clonal extinction of oncogenic *BRAF*^{V600E} clones (fig 2j). Lastly, the findings also highlight that stochastic selection of oncogenic mutations is modulated by the adaptive immune system.

Tregs promote extinction of BRAF^{V600E} mutant clones

MHCII expression on the small intestinal epithelial stem cells, expand CD4+ T cells in the stem cell microenvironment during infection[26]. To investigate if *MHCII* expression on BRAF^{V600E} mutated colonic stem cells similarly expand CD4+ T cell population, we generated an immune-enriched (CD45+), colonic, single cells data set following epithelial *BRAF*^{V600E} induction (fig. 3a, extended fig. 3b). The population of professional antigen presentation immune cells (monocyte/macrophages, B cells and dendritic cells) were depleted; however, a dramatic expansion of effector and more crucially regulatory T lymphocytes was noted (fig. 3b) in the *BRAF*^{V600E} mutated colon. These findings are consistent with T cell enrichment and myeloid cell exclusion noted in BRAF^{V600E} mutated colon cancers[28,42]. Furthermore, a significant enrichment of T cell activation and differentiation pathways (fig. 3c) in the *BRAF*^{V600E} mutant colonic immune cells was observed. In addition to expansion of the Treg population, a significant upregulation of Treg activation genes (*Tgfb1*, *Gzmb*, *Tnfrsf18*, *CD39*, *CD137*, *Ctla4* and *Helios*) and concomitant downregulation of negative regulators of Tregs (*Stat1*, *Fos* and *Jun*) was also noted in Tregs from *BRAF*^{V600E} mutated colon (fig. 3d).

Intestinal stem cell fate is primarily regulated by developmental Wnt, BMP, YAP and Notch pathway signals emanating from the niche mesenchymal cells [43–46]. Analogous to the mesenchymal cells, CD4+ T cells are also crucial for determination of stem cell fate via their effector cytokines[26]. Amongst the CD4+ cells, Tregs exclusively expand healthy intestinal progenitor population[26]. Conversely, Treg depletion leads to depletion of healthy stem cells[26]. Role of Tregs in intestinal carcinogenesis is complicated, with studies highlighting both promotion and restriction of tumor growth of intestinal tumors by Tregs[9,47]. Their role in crypt fixation of oncogene is not known. To investigate the impact of Tregs expansion, observed in our single cell analysis, on fixation or extinction of *BRAF*^{V600E} clones, we crossed our *BRAF*^{V600E}*; VillinCre*^{ERT} mice with an establish genetic model of Treg depletion, *Foxp3*^{DTR} mice (fig. 3e). This allowed us to specifically and acutely deplete Tregs during the clonal selection of *BRAF*^{V600E} mutant cells by diphteria toxin (DT) administration (fig. 3e). *BRAF*^{V600E} mutant clones in Treg depleted mice showed significantly increased crypt fixation, compared to *BRAF*^{V600E} clones in Treg competent mice (fig. 3f-g). Under the standard assumptions of SCB model (k_r = 0.0525 and k_d = 0.21), we inferred that the self-replication rate of BRAF^{V600E} mutant cells increased to k_d^{μ} = 0.73 from 0.51 in Treg depleted mice (extended fig. 3a). Likewise, the probability of *BRAF*^{V600E} mutants replacing their WT neighbors in the absence of Tregs was also significantly higher (0.802 ± 0.049), compared to (0.726 ± 0.058) in mice with intact Tregs (fig. 3h). Lastly, *BRAF*^{V600E} mutant clones are more effective in fixing colonic crypts (extended fig. 4b) with a significantly lower probability of clonal extinction (0.345 ± 0.049), compared to Treg competent mice (0.479 ± 0.050) (fig. 3i). These experiments, for the first time, provide quantifiable evidence of the impact of a specific

microenvironment cell on the clonal competition for crypt fixation and a novel mechanism to eliminate cancerous stem cells. Overall, these findings highlight a critical role of Tregs in promoting extinction of *BRAF*^{V600E} mutant clones.

Epithelial IL10RA promote extinction of BRAF^{V600E} Clones.

Tregs perform their primary functions through its effector cytokine interleukin 10 (IL10) that specifically binds to its receptor, interleukin 10RA (IL10RA) on the target cells[47,48]. To investigate if clonal extinction of *BRAF*^{V600E} mutant cells is mediated via Il10RA, we first administered anti-IL10RA antibody to our mouse model during the clonal competition (fig. 4a). Compared to isotype control, *BRAF*^{V600E} mutated clones in anti-IL10RA treated mice showed a significant increase in percent fixed clones (fig 4b-c). By contrast, treatment of WT confetti mice with anti-IL10RA showed no significant increase in clonal fixation (fig 4b-c). Under the standard assumptions (k_r = 0.0525 and k_d = 0.21), we inferred that the self-replication rate of *BRAF*^{V600E} mutant cells increased to $k_d{}^{\mu}$ = 0.59 in anti-Il10RA treated mice compared to $k_d{}^{\mu}$ = 0.44 in the isotype controls (extended fig. 4b fig.). Likewise, the probability of *BRAF*^{V600E} mutants replacing their WT neighbors in the anti-IL10RA treated mice was also significantly higher (0.78 ± 0.05), compared to (0.69 ± 0.06) in isotype control treated mice (extended fig. 3d)

IL10RA is expressed predominantly on the immune cells targeted by Tregs in addition to the epithelial cells[26,48]. This raises the question that the impact of Treg depletion or IL10RA blocking on clonal extinction of *BRAF*^{V600E} clones, is through direct targeting of the mutant clones or regulation of other cells on the microenvironment, that can also potentially influence crypt fixation. To isolate the impact of IL10RA blocking on the mutant clones alone, we crossed *BRAF*^{V600E}*; VillinCre*^{ERT2} mice with *IL10RA*$^{fl/fl}$ mice

(fig. 4e). This allows specific deletion of IL10RA on the *BRAF*^{V600E} mutated cells while preserving its expression on adjacent WT epithelial cells as well as non-epithelial cell in the stem cell microenvironment (fig. 4e). Loss of IL10RA in our *BRAF*^{V600E}*; IL10RA*$^{fl/fl}$ mice showed significant increase in the rate of crypt fixation when compared to BRAF^{V600E} clones with intact IL10RA (*BRAF*$^{V600E;}$*IL10RA*$^{fl/fl}$) (fig. 4f-g). Keeping the standard assumptions as before, we inferred that the division rate for *BRAF*^{V600E}*; IL10RA* deficient clones was increased to ($k_d{}^{\mu}$ = 0.6) than the IL10RA intact *BRAF*^{V600E} clones ($k_d{}^{\mu}$ = 0.44) (fig. 4g). Thus, loss of IL10RA expression, significantly increased the probability of these clones to replace their WT neighbors (0.76 ± 0.05) compared to *BRAF*^{V600E} clones with intact IL10RA expression (0.69 ± 0.06) (extended fig 4e). This results in a higher likelihood of crypt fixation (extended fig. 4d) and a significant reduction in the extinction of *BRAF*^{V600E} clones to following loss of IL10RA (0.42 ± 0.051), compared to clones with intact IL10RA expression (0.54 ± 0.048) (fig. 4h).

Overall, we highlight a new immune sensing mechanism that eradicates oncogene mutant stem cells from the colon using a combination of in-vivo systems and theoretical modeling. Strikingly, this surveillance acts at the very first event following cancer mutagenesis. Our work showed that Tregs sense oncogene mutated stem cell clones via selective expression of MHCII and induce extinction of these mutant clones in an IL10RA dependent manner (fig. 4i). We highlight that the clonal extinction is an active process and show for the first time that a microenvironment cell can impacts competition between WT and precancerous cells prior to crypt fixation.

Discussion:

Our work builds on the conceptual framework of immune surveillance provided by Burnet and Thomas in the 1950s[49,50]. They proposed active elimination of nascent tumor cells by the immune system in pre-malignant tissue[49,50]. This framework is considered the foundation of modern immunooncology[50] and resulted in development of remarkably successful immunotherapies for late-stage cancers[30]. Relevance of immunosurveillance in precancerous tissues remains poorly understood, due to lack of appropriate experimental models that can dissect the impact of immune system on the stochastic processes of tumor initiation. Moreover, stem cells were previously believed to be outside the purview of immunosurveillance owing to their purported immune privilege status[51], and intestinal stem cell dynamics were previously believed to be regulated exclusively by developmental signals from the mesenchymal niche. Here we reveal a previously unrecognized contribution of the adaptive immune system in the extinction of oncogenic stem cells prior to their fixation, an essential and early milestone for tumor initiation.

Unlike advanced cancers, where Treg suppresses the targeted killing of tumor cells[47], in our work, Tregs induce targeted extinction of oncogenic clones at tumor initiation, performing a previously unknown immune sensing function. Tregs performs this function by specifically identifying the mutant clones, which uniquely express *MHCII*, and suppress the clonal progression of these oncogenic clones via engagement of *Il10RA*. This is a highly effective strategy that eliminates the majority of oncogenic clones and future work on these mechanisms of tumor suppressive function may provide novel ways to prevent rather than only treat established cancer.

The work raises several new questions. Helper T cell and CD8 positive T cells, other components of adaptive immune system were also heavily recruited to the

BRAF^{V600E} mutant cells. Moreover, the adaptive immune system not only interacts with the stem cells but may also impact the mesenchymal cells in the stem cell niche. Experimental and theoretical model systems presented in this study will be crucial in investigating how these complex multi-cell interactions impact elimination of deleterious oncogenic clones by extinction and will provide additional avenues to unravel the immune prevention strategies.181825[47]

Methods

Mice

All inducible Cre lines (*Villin-CreERT2*: JAX020282; *CDX2-CreERT2*: 022390), the *R26R-Confetti* line (JAX017492), the *LSL-BRAF*^{V600E} (JAX017837) line, the *MHCII*$^{fl/fl}$ line (JAX037739), thee IL10RA$^{fl/fl}$ line (JAX028146) and the *Foxp3*^{DTR} line (JAX016958) were obtained from The Jackson Laboratory. All these mice were bred in the facilities of the Yale Animal Resources Center and were maintained on a C57BL/6J genetic background. Mice were used for experiments at 8–12 weeks of age unless otherwise indicated. For all experiments, littermate, co-housed and sex-matched mice were used. Both male and female mice were used for experiments. No mice were excluded from the analyses performed. End points used for mice developing tumors were changes in activity or mobility, abnormal posture, decreased food and/or water intake and decreased body temperature. All animal experimentation at Yale was performed in compliance with Yale Institutional Animal Care and Use Committee protocols.

Animal treatments

To perform lineage tracing, tamoxifen (Sigma, T5648) dissolved in corn oil was injected intraperitoneally into 8–12-week-old mice. As indicated, the dose of tamoxifen used for each experiment was determined on the basis of recombination efficiency. For the clonal analysis, it is crucial that crypts are marked at clonal density so that labelled cells can be identified reliably as the output of an individual labelled cell. Titration experiments indicated that this can be achieved by a tamoxifen dose of 0.2 mg per 20 g mouse body weight. Deletion of $Foxp3^{+}$ Treg was performed by IP administration of 10 μg Diphtheria toxin (Sigma, D0564) per kg body weight.

Tissue processing and quantification of clone sizes

After the mice were killed, intestines were removed fully and washed thoroughly with ice-cold PBS. The intestines were opened longitudinally and fixed for 2 hours in 4% paraformaldehyde (PFA) solution. To preserve tissue integrity, the intestines were kept in 30% sucrose solution overnight before freezing. Crypt bases were sliced with a thickness of 10 μm using a Cryostat NX70 cryostat and placed on glass slips and counterstained with DAPI with fluoroshield (Sigma, F6057). Fluorescent lineage tracing labels were visualized with BZ-X1000 microscope (Keyance). For all crypt analyses, clone sizes were quantified as proportions of the crypt circumference (in eights, 1:8 to 8:8) by an expert gastrointestinal pathologist.

Single cell RNA sequencing

Intestinal tissues were harvested and separated surgically to isolate proximal colon. These tissues were then cleaned to remove excess fat lining and turned inside out to expose lumen. Intestines were then treated with RPMI containing 1 mM DTT, 20 mM

EDTA and 2% FBS at 37C for 15 min to remove epithelial cells and lymphocytes residing in the epithelium. Single cell suspensions present in the supernatant were then filtered and washed with 4% RPMI. These cells were then spun fown at 1500 rpmi for 10 min. The remaining intestinal mucosa encompassing lamina propria was washed, minced and dissociated in collagenase solution(1.5mg/ml collagenase II (Gibco), 0.5mg/ml dispase and 1%FBS in RPMI) with constantly stirring at 37oC for 30-45min. Single cell suspensions were then filtered and washed with 4% RPMI solution. Epithelial and lamina propria cells were then pooled before proceeding with 10X Chromium protocols. Intestinal cells were loaded onto the 10x Chromium Controller using the Chromium Next GEM technology. Library preparation was performed in-house using the Chromium Next GEM Single Cell 3' Reagent Kits v3.1 (10x Genomics), including cell surface feature barcoding. Sequencing was conducted on the NovaSeq 6000 system (Illumina).Raw sequencing data were processed using Cell Ranger (v7.1.0). The filtered feature-barcode matrix from Cell Ranger was analyzed in R (v4.2.3) using Seurat (v5.0.1).

Statistical analysis

All in vivo histological data were scored blindly. Visualization and statistical analysis of data were performed using GraphPad Prism, in which most data were analyzed using two-sided Student's *t*-test. In case other statistical tests were applied, this was noted in the figure legends.

References:

1. Vermeulen L, Morrissey E, Heijden M van der, et al. Defining Stem Cell Dynamics in Models of Intestinal Tumor Initiation. Science (1979) 2013;342:995–998.

2. Snippert HJ, Schepers AG, Es JH, et al. Biased competition between Lgr5 intestinal stem cells driven by oncogenic mutation induces clonal expansion. EMBO Rep 2013;15:62–69.

3. Vermeulen L, Snippert HJ. Stem cell dynamics in homeostasis and cancer of the intestine. Nature Publishing Group 2014. Available at: www.nature.com/reviews/cancer.

4. Ramadan R, Driel MS van, Vermeulen L, et al. Intestinal stem cell dynamics in homeostasis and cancer. Trends Cancer 2022;8:416–425.

5. Kozar S, Morrissey E, Nicholson AM, et al. Continuous clonal labeling reveals small numbers of functional stem cells in intestinal crypts and adenomas. Cell Stem Cell 2013;13:626–633.

6. Driel MS van, Linssen JDG, Flanagan DJ, et al. Caffeine Limits Expansion of Apc-Deficient Clones in the Intestine by NOTUM Inhibition. CMGH 2023;16.

7. Yum MK, Han S, Fink J, et al. Tracing oncogene-driven remodelling of the intestinal stem cell niche. Nature 2021;594:442–447. Available at: http://dx.doi.org/10.1038/s41586-021-03605-0.

8. Sadien ID, Adler S, Mehmed S, et al. Polyclonality overcomes fitness barriers in Apc-driven tumorigenesis. Nature 2024;634:1196–1203.

9. Huang X, Feng D, Mitra S, et al. Opposing Functions of Distinct Regulatory T Cell Subsets in Colorectal Cancer. bioRxiv 2025.

10. Azkanaz M, Corominas-Murtra B, Ellenbroek SIJ, et al. Retrograde movements determine effective stem cell numbers in the intestine. Nature 2022.

11. Corominas-Murtra B, Scheele CLGJ, Kishi K, et al. Stem cell lineage survival as a noisy competition for niche access. Proc Natl Acad Sci U S A 2020;117:16969–16975. Available at: https://pubmed.ncbi.nlm.nih.gov/32611816/ [Accessed September 14, 2020].

12. Neerven SM van, Groot NE de, Nijman LE, et al. Apc-mutant cells act as supercompetitors in intestinal tumour initiation. Nature 2021.

13. Fischer JM, Schepers AG, Clevers H, et al. Occult progression by Apc-deficient intestinal crypts as a target for chemoprevention. Carcinogenesis 2014;35:237–246.

14. Flanagan DJ, Pentinmikko N, Luopajärvi K, et al. NOTUM from Apc-mutant cells biases clonal competition to initiate cancer. Nature 2021.

15. Yum MK, Han S, Fink J, et al. Tracing oncogene-driven remodelling of the intestinal stem cell niche. Nature 2021.

16. Nicholson AM, Olpe C, Hoyle A, et al. Fixation and Spread of Somatic Mutations in Adult Human Colonic Epithelium. Cell Stem Cell 2018;22:909-918.e8.

17. Olpe C, Khamis D, Chukanova M, et al. A Diffusion-like Process Accommodates New Crypts During Clonal Expansion in Human Colonic Epithelium. Gastroenterology 2021.

18. Schepers AG, Snippert HJ, Stange DE, et al. Lineage Tracing Reveals Lgr5+ Stem Cell Activity in Mouse Intestinal Adenomas. Science (1979) 2012;337:730–735. Available at: https://www.sciencemag.org/lookup/doi/10.1126/science.1224676.

19. HJ S, LG van der F, T S, et al. Intestinal crypt homeostasis results from neutral competition between symmetrically dividing Lgr5 stem cells. Cell 2010;143:134–44. Available at: http://www.ncbi.nlm.nih.gov/pubmed/20887898.

20. Colozza G, Park SY, Koo BK. Clone wars: From molecules to cell competition in intestinal stem cell homeostasis and disease. Experimental & Molecular Medicine 2022 54:9 2022;54:1367–1378. Available at: https://www.nature.com/articles/s12276-022-00854-5 [Accessed January 15, 2026].

21. Shahriyari L, Komarova NL, Jilkine A. The role of cell location and spatial gradients in the evolutionary dynamics of colon and intestinal crypts. Biol Direct 2016;11:42-. Available at: https://link.springer.com/article/10.1186/s13062-016-0141-6 [Accessed January 15, 2026].

22. Quintero M, Samuelson LC. Paneth Cells: Dispensable yet Irreplaceable for the Intestinal Stem Cell Niche. CMGH 2025;19.

23. Roulis M, Kaklamanos A, Schernthanner M, et al. Paracrine orchestration of intestinal tumorigenesis by a mesenchymal niche. 524 | Nature | 2020;580. Available at: https://doi.org/10.1038/s41586-020-2166-3.

24. Roulis M, Flavell RA. Fibroblasts and myofibroblasts of the intestinal lamina propria in physiology and disease. Differentiation 2016;92:116–131. Available at: http://dx.doi.org/10.1016/j.diff.2016.05.002 [Accessed September 20, 2020].

25. Goto N, Goto S, Imada S, et al. Lymphatics and fibroblasts support intestinal stem cells in homeostasis and injury. Cell Stem Cell 2022;29.

26. Biton M, Haber AL, Rogel N, et al. T Helper Cell Cytokines Modulate Intestinal Stem Cell Renewal and Differentiation. Cell 2018;175:1307-1320.e22.

27. Agudo J, Park ES, Rose SA, et al. Quiescent Tissue Stem Cells Evade Immune Surveillance. Immunity 2018;48:271-285.e5.

28. Chen B, Scurrah CR, McKinley ET, et al. Differential pre-malignant programs and microenvironment chart distinct paths to malignancy in human colorectal polyps. Cell 2021;184:6262-6280.e26.

29. Goto N, Westcott PMK, Goto S, et al. SOX17 enables immune evasion of early colorectal adenomas and cancers. Nature 2024;627.

30. Cercek A, Lumish M, Sinopoli J, et al. PD-1 Blockade in Mismatch Repair–Deficient, Locally Advanced Rectal Cancer. New England Journal of Medicine 2022;386:2363–2376. Available at: https://www.nejm.org/doi/full/10.1056/NEJMoa2201445 [Accessed January 15, 2026].

31. Mendiratta G, Ke E, Aziz M, et al. Cancer gene mutation frequencies for the U.S. population. Nat Commun 2021;12.

32. Marty Pyke R, Thompson WK, Salem RM, et al. Evolutionary Pressure against MHC Class II Binding Cancer Mutations. Cell 2018;175:416-428.e13.

33. Morkel M, Riemer P, Bläker H, et al. Similar but different: Distinct roles for KRAS and BRAF oncogenes in colorectal cancer development and therapy resistance. Oncotarget 2015;6.

34. Azkanaz M, Corominas-Murtra B, Ellenbroek SIJ, et al. Retrograde movements determine effective stem cell numbers in the intestine. Nature 2022.

35. Tang R, Sansonetti PJ, Gao YZ. Stem cell retrograde: A new reason why colorectal cancer is more common than small intestinal cancer? Innovation 2023;4.

36. Tong K, Kothari OA, Haro KS, et al. SMAD4 is critical in suppression of BRAF-V600E serrated tumorigenesis. Oncogene 2021;40:6034–6048.

37. Hisamatsu K, Noguchi K, Tomita H, et al. Distinctive crypt shape in a sessile serrated adenoma/polyp: Distribution of Ki67-, p16INK4a-, WNT5A-positive cells and intraepithelial lymphocytes. Oncol Rep 2017;38.

38. Lopez-Garcia C, Klein AM, Simons BD, et al. Intestinal Stem Cell Replacement Follows a Pattern of Neutral Drift. Science (1979) 2010;330:822–825. Available at: https://www.sciencemag.org/lookup/doi/10.1126/science.1196236.

39. Snippert HJ, Schepers AG, Es JH, et al. Biased competition between Lgr5 intestinal stem cells driven by oncogenic mutation induces clonal expansion. EMBO Rep 2013;15:62–69.

40. Koyama M, Mukhopadhyay P, Schuster IS, et al. MHC Class II Antigen Presentation by the Intestinal Epithelium Initiates Graft-versus-Host Disease and Is Influenced by the Microbiota. Immunity 2019;51:885-898.e7.

41. Lavalou J, Kulakova K, Subramaniam YJ, et al. Mechanisms of cellular fitness and cell competition: Towards an integrated view. Curr Opin Cell Biol 2025;96.

42. Marteau V, Nemati N, Handler K, et al. Single-cell integration and multi-modal profiling reveals phenotypes and spatial organization of neutrophils in colorectal cancer. bioRxiv 2025;16.

43. Morrison SJ, Spradling AC. Leading Edge Review Stem Cells and Niches: Mechanisms That Promote Stem Cell Maintenance throughout Life.

44. Gehart H, Clevers H. Tales from the crypt: new insights into intestinal stem cells. Nat Rev Gastroenterol Hepatol. Available at: https://doi.org/10.1038/.

45. Serra D, Mayr U, Boni A, et al. Self-organization and symmetry breaking in intestinal organoid development. Nature 2019;569.

46. Choi J, Augenlicht LH. Intestinal stem cells: guardians of homeostasis in health and aging amid environmental challenges. Exp Mol Med 2024;56.

47. Yu H, Yang R, Li M, et al. The role of Treg cells in colorectal cancer and the immunotherapy targeting Treg cells. Front Immunol 2025;16.

48. Shevyrev D, Tereshchenko V. Treg Heterogeneity, Function, and Homeostasis. Front Immunol 2020;10:3100. Available at: www.frontiersin.org [Accessed November 18, 2020].

49. Burnet SM. Cancer - A biological approach. Br Med J 1957;1.

50. Ribatti D. The concept of immune surveillance against tumors. The first theories. Oncotarget 2017;8.

51. Galassi C, Musella M, Manduca N, et al. The immune privilege of cancer stem cells: A key to understanding tumor immune escape and therapy failure. Cells 2021;10.

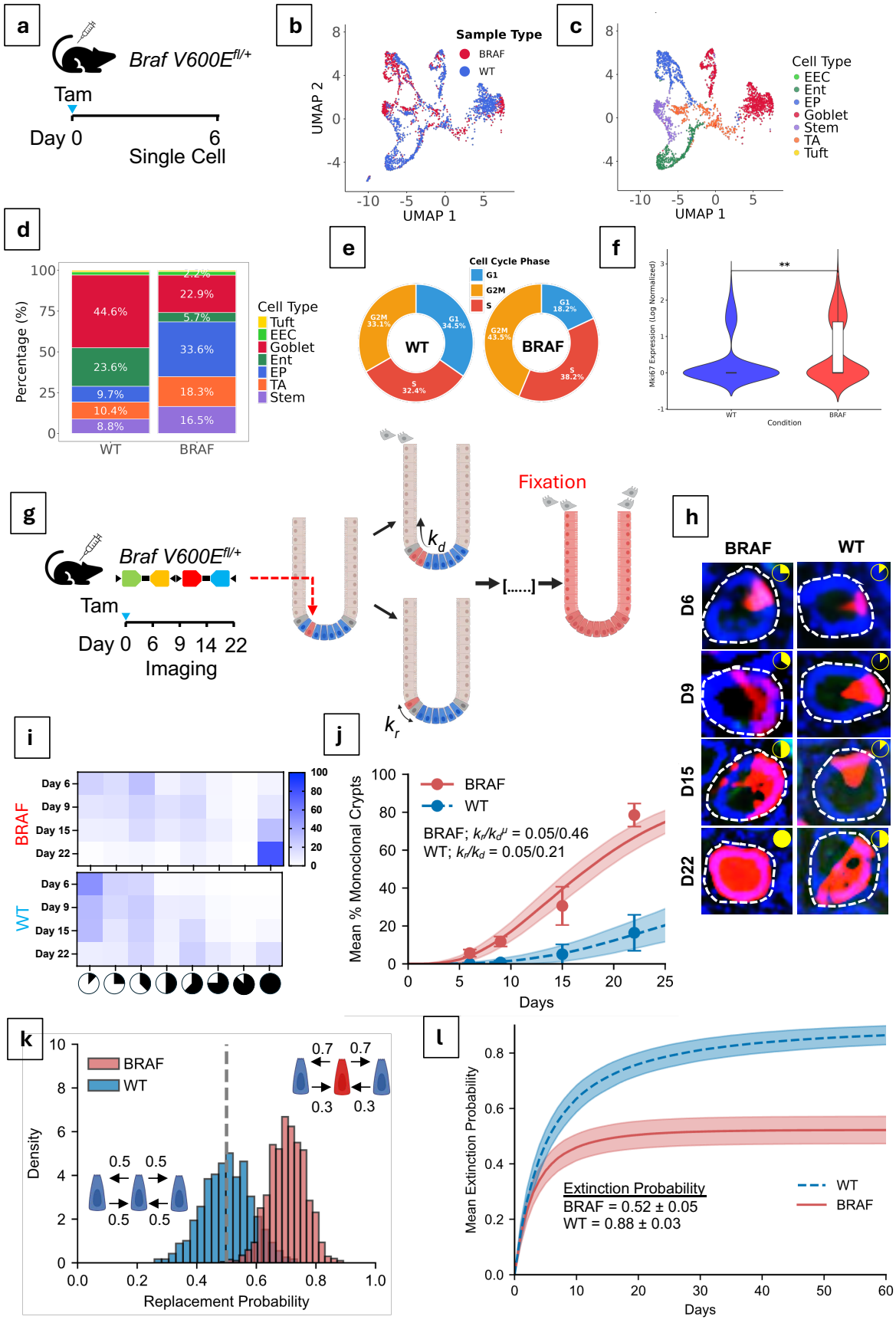

a
Braf V600E fl/+
Tam
Day 0
6
Single Cell
b
Sample Type
BRAF
WT
UMAP 2
UMAP 1
c
Cell Type
EEC
Ent
EP
Goblet
Stem
TA
Tuft
UMAP 1
d
Percentage (%)
44.6%
23.6%
9.7%
10.4%
8.8%
2.2%
22.9%
5.7%
33.6%
18.3%
16.5%
WT
BRAF
Cell Type
Tuft
EEC
Goblet
Ent
EP
TA
Stem
e
Cell Cycle Phase
G1
G2M
S
WT
G1 34.5%
S 32.4%
G2M 33.1%
BRAF
G1 18.2%
S 38.2%
G2M 43.5%
f
Mki67 Expression (Log Normalized)
**
WT
BRAF
Condition
g
Braf V600E fl/+
Tam
Day 0 6 9 14 22
Imaging
Fixation
[.....]
h
BRAF
WT
D6
D9
D15
D22
i
BRAF
WT
Day 6
Day 9
Day 15
Day 22
j
BRAF
WT
BRAF; kr/kd^μ = 0.05/0.46
WT; kr/kd = 0.05/0.21
Mean % Monoclonal Crypts
Days
k
BRAF
WT
Density
0.7 0.7
0.3 0.3
0.5 0.5
0.5 0.5
Replacement Probability
l
Mean Extinction Probability
Extinction Probability
BRAF = 0.52 ± 0.05
WT = 0.88 ± 0.03
WT
BRAF
Days

Figure 1: Fixation of colonic crypts by BRAF V600E mutation via biased drift.

a, Schematic showing experimental design of mouse model for colonic epithelial single cell analysis following induction of BRAF V600E$^{fl/+}$ mutation using inducible VillinCre^{ERT2} model.

b and c, Uniform manifold approximation and projection (UMAP) plot showing clustering of epithelial cells based on marker expression: stem cells (Stem), transit-amplifying (TA) cells, enterocyte progenitors (EP), Enterocytes (Ent), enteroendocrine cells (EEC), goblet cells and tuft cells.

d, Percentage of different epithelial cell types in *BRAF V600E*$^{fl/+}$ and control mice

e, Graph depicting percentage of stem cells at cell cycle phases G1, G2M and S phases.

f, Violin plot highlighting Ki67 expression in the WT and BRAF V600E mutated stem cells, ** denotes *p*-value <0.001 (Wilcoxon test)

g, Schematic showing combination of experimental design of low-dose, inducible mutagenesis using ubiquitous epithelial VillinCre^{Ert2} inducible cre recombinase system and the theoretical model of stochastic (SCB) conveyor belt. k_d is the cell division rate, leading to upward movement of cells and k_r is the random cell relocation rate, including retrograde movements.

h, Representative confocal images of colonic crypt bottoms of *WT* and BRAF V600E-mutated, VillinCre^{ERT2}; Confetti mice at the indicated time points after clone induction. Clone sizes are indicated as fractions (in eighths) of the crypt circumference. Blue, nuclear stain (DAPI); red, RFP+ clones in confetti mice.

i, Heat maps depict the frequency of clones of the indicated size (columns) at indicated time points (rows) for both WT and BRAF V600E (left).

j, Probability of % of fixed clones over time as predicted by the SCB model (line ± s.d. as shaded area) and % of fixed clones in experimental data (dots) for WT and BRAF V600E mice after tamoxifen induction (right). *n* = 5 mice per genotype per time point with at least 100 clones examined per mice. Data (dots) are mean ± s.d. of mean.

k, Inference of the biased drift parameter (replacement probability) for WT vs WT and BRAF V600E vs WT clones. The vertical axis indicates probability density. Cartoon summarizes the replacement properties (with color coding as in the graph).

l, Graph depicts the likelihood of extinction of the indicated clone types. Shaded areas indicate ± s.d. The extinction probability of clones is indicated in the figure (value at 100 days).

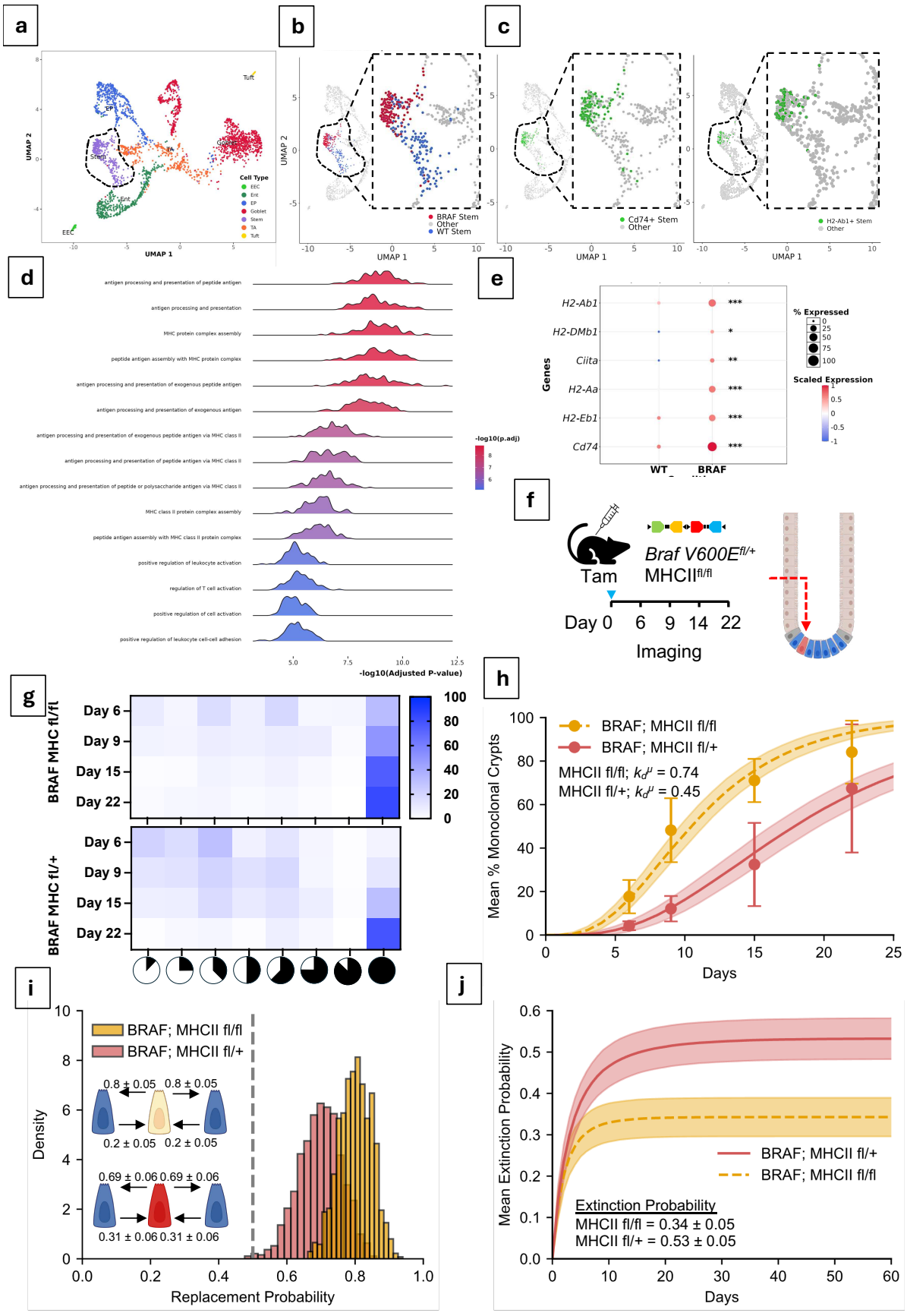

a
b
c
d
e
f
g
h
i
j
UMAP 1
UMAP 2
Cell Type
EEC
Ent
EP
Goblet
Stem
TA
Tuft
BRAF Stem
Other
WT Stem
Cd74+ Stem
H2-Ab1+ Stem
antigen processing and presentation of peptide antigen
antigen processing and presentation
MHC protein complex assembly
peptide antigen assembly with MHC protein complex
antigen processing and presentation of exogenous peptide antigen
antigen processing and presentation of exogenous antigen
antigen processing and presentation of exogenous peptide antigen via MHC class II
antigen processing and presentation of peptide antigen via MHC class II
antigen processing and presentation of peptide or polysaccharide antigen via MHC class II
MHC class II protein complex assembly
peptide antigen assembly with MHC class II protein complex
positive regulation of leukocyte activation
regulation of T cell activation
positive regulation of cell activation
positive regulation of leukocyte cell-cell adhesion
-log10(p.adj)
-log10(Adjusted P-value)
H2-Ab1
H2-DMb1
Ciita
H2-Aa
H2-Eb1
Cd74
Genes
WT
BRAF
% Expressed
Scaled Expression
Tam
Braf V600E fl/+
MHCII fl/fl
Day 0 6 9 14 22
Imaging
BRAF MHC fl/fl
BRAF MHC fl/+
Day 6
Day 9
Day 15
Day 22
BRAF; MHCII fl/fl
BRAF; MHCII fl/+
MHCII fl/fl; k_d^{μ} = 0.74
MHCII fl/+; k_d^{μ} = 0.45
Mean % Monoclonal Crypts
Days
Density
0.8 ± 0.05
0.2 ± 0.05
0.69 ± 0.06
0.31 ± 0.06
Replacement Probability
Mean Extinction Probability
Extinction Probability
MHCII fl/fl = 0.34 ± 0.05
MHCII fl/+ = 0.53 ± 0.05

Figure 2: MHCII expression suppress clonal fixation of BRAF V600E mutant clones

a-c, Combined UMAP highlighting increased expression of MHCII pathway genes in and $BRAF^{V600E}$ mutated epithelial stem cells. Stem cell cluster highlighted in purple, encircled by lasso (a).

b, BRAF V600E mutated stem cells form a distinct cluster (red) adjacent to the WT stem cell cluster (blue).

c, Expression of MCHII pathway genes (green), CD74 and H2Ab1 are restricted to the the BRAF V600E stem cell and absent from the WT stem cell cluster.

d, Ridgeplots highlighting enrichment of genes (upregulated in $BRAF^{V600E}$ mutated stem cells compared to WT stem cells, in selected GO terms identified through Gene Set Enrichment Analysis (GSEA). The y-axis lists the top enriched GO biological process terms, ordered by significance (lowest adjusted p-value). The color gradient of the ridges corresponds to the adjusted p-value.

e, Dotplot highlighting increased expression of MHCII pathway related genes in BRAF V600E mutated stem cells * denotes *p*-value <0.001 (Wilcoxon test)

f, Schematic showing experimental design of low-dose, inducible BRAF V600E mutagenesis with concurrent clonal MHCII deletion.

g, Heat maps depicting the frequency of clones of the indicated size (columns) at various time points (rows) for both BRAF V600E;$MHCII^{fl/+}$ and BRAF V600E;$MHCII^{fl/fl}$ clones.

h, Probability of % of fixed clones over time as predicted by the SCB model (line with ± s.d. as shaded area) and % of fixed clones in experimental data (dots) for BRAF V600E;$MHCII^{fl/+}$ and BRAF V600E;$MHCII^{fl/fl}$ mice after tamoxifen induction (right). n = 5 mice per genotype per time point with at least 100 clones examined per mice. Data (dots) are mean ± s.d. of mean.

i, Bayesian inference of the biased drift parameter (replacement probability) for BRAF V600E;$MHCII^{fl/+}$ and BRAF V600E;$MHCII^{fl/fl}$ clones. The vertical axis indicates probability density. Cartoon summarizes the replacement properties (blue=WT with color coding as in the graph).

j, Graph highlights the likelihood of extinction of indicated clone types. Shaded areas indicate ± s.d. The extinction probabilities are indicated in the figure (value at 100 days).

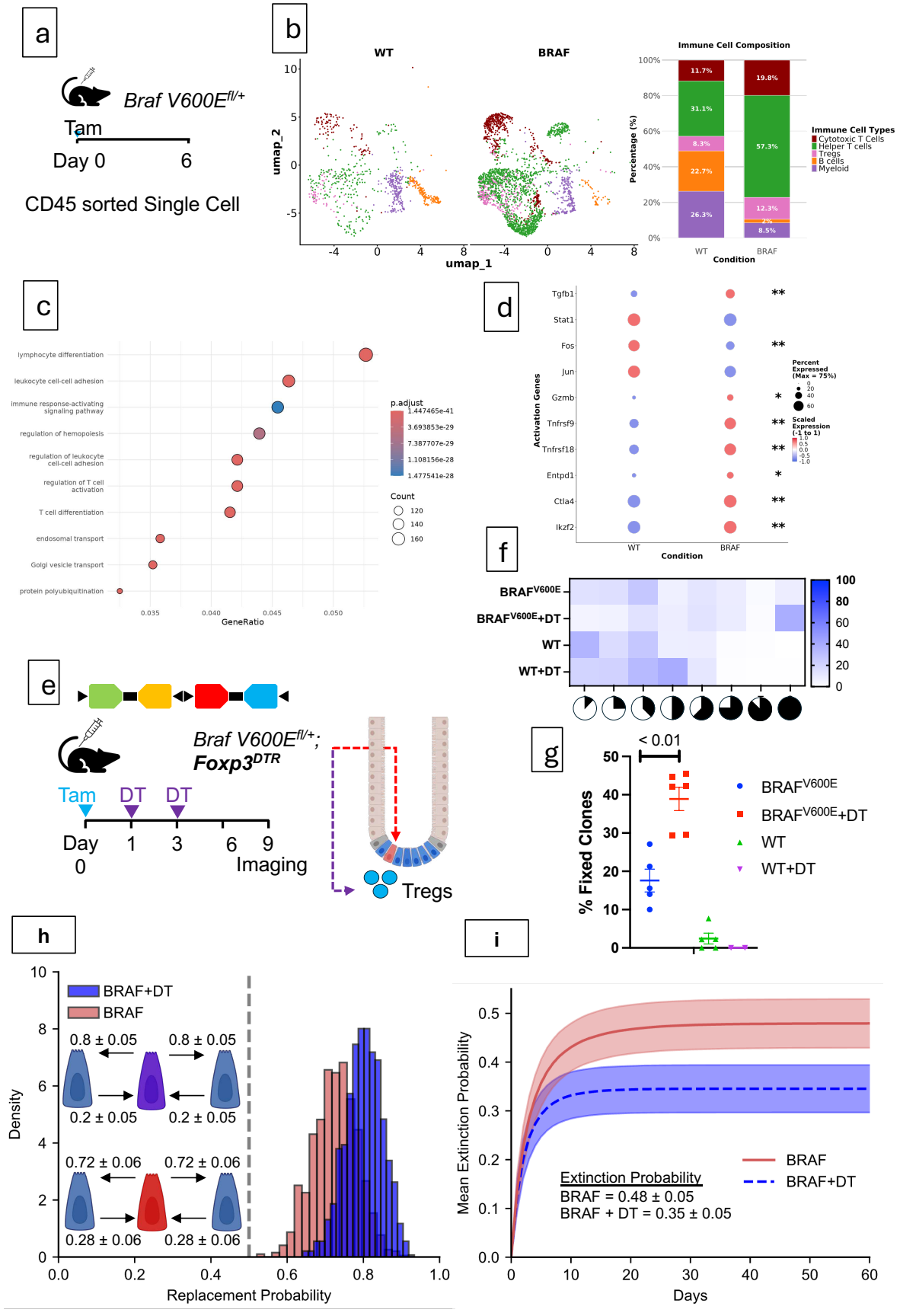

a
Braf V600E fl/+
Tam
Day 0
6
CD45 sorted Single Cell
b
WT
BRAF
umap_2
umap_1
Immune Cell Composition
Percentage (%)
Condition
Immune Cell Types
Cytotoxic T Cells
Helper T cells
Tregs
B cells
Myeloid
11.7%
31.1%
8.3%
22.7%
26.3%
19.8%
57.3%
12.3%
2%
8.5%
c
lymphocyte differentiation
leukocyte cell-cell adhesion
immune response-activating signaling pathway
regulation of hemopoiesis
regulation of leukocyte cell-cell adhesion
regulation of T cell activation
T cell differentiation
endosomal transport
Golgi vesicle transport
protein polyubiquitination
GeneRatio
p.adjust
Count
d
Tgfb1
Stat1
Fos
Jun
Gzmb
Tnfrsf9
Tnfrsf18
Entpd1
Ctla4
Ikzf2
Activation Genes
Percent Expressed (Max = 75%)
Scaled Expression (-1 to 1)
Condition
e
Braf V600E fl/+;
Foxp3 DTR
Tam
DT
DT
Day 0
1
3
6
9
Imaging
Tregs
f
BRAF V600E
BRAF V600E +DT
WT
WT+DT
g
< 0.01
% Fixed Clones
BRAF V600E
BRAF V600E +DT
WT
WT+DT
h
BRAF+DT
BRAF
0.8 ± 0.05
0.2 ± 0.05
0.72 ± 0.06
0.28 ± 0.06
Density
Replacement Probability
i
Mean Extinction Probability
Days
Extinction Probability
BRAF = 0.48 ± 0.05
BRAF + DT = 0.35 ± 0.05
BRAF
BRAF+DT

Figure 3: Tregs suppress *BRAF^{V600E}* selection.

a, Schematic showing experimental design of mouse model for colonic immune cel (CD45+) single cell analysis following induction of BRAF V600E mutation using inducible VillinCre^{ERT2} model.

b, UMAP plot showing clusters of immune cells in WT and BRAF V600E mutated colon (left). Percentage of different immune cell types in BRAF V600E and control mice (right)

c, Dotplot highlighting enrichment of genes in immune cells (upregulated in BRAFV600E mutated colon compared to WT), in selected GO terms identified through Gene Set Enrichment Analysis (GSEA). The y-axis lists the top enriched GO biological process terms, ordered by significance (lowest adjusted p-value). The color gradient of the ridges corresponds to the adjusted p-value.

d, Dotplot highlighting expression of Treg activation genes from the colon harboring BRAF V600E mutated stem cells. * denotes *p*-value <0.001 (Wilcoxon test)

e, Schematic showing experimental design of low-dose, inducible mutagenesis with concurrent depletion of Tregs in BRAFV600E; VillinCre^{ERT}; Foxp3^{DTR} mice

f, Heat map depicts the relative frequency of clones of the indicated size (columns) in various conditions (rows) for both BRAFV600E and WT clones in the presence or absence of Diphtheria toxin (DT) treatment.

g, Dotplot depicting % of fixed clones for BRAF V600E and WT mice in the presence or absence of Tregs. Each dot represent a mouse with at least 100 clones examined per mice. Error bars represent s.d. of mean.

h, Bayesian inference of the biased drift parameter (replacement probability) for BRAFV600E clones in the presence or absence of Tregs. The vertical axis indicates probability density. Cartoon summarizes the replacement properties (color coding as in the graph).

i, Graph highlights the likelihood of the indicated clone types reaching fixation in a crypt over time. Shaded areas indicate ± s.d. The fixation probabilities are indicated in the figure (value at 100 days).

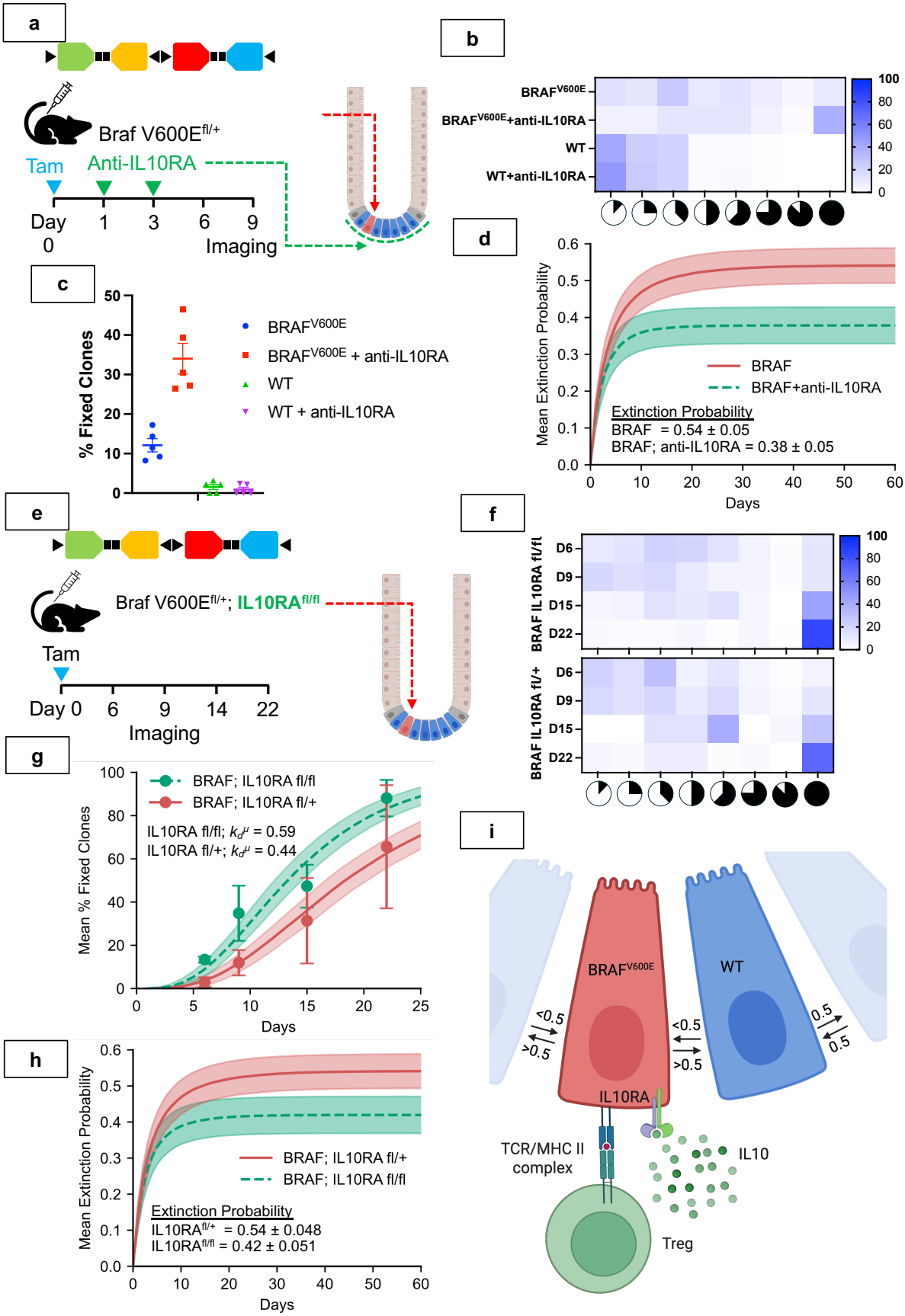

a
Braf V600E fl/+
Tam
Anti-IL10RA
Day 0 1 3 6 9
Imaging
b
BRAF V600E
BRAF V600E +anti-IL10RA
WT
WT+anti-IL10RA
100 80 60 40 20 0
c
% Fixed Clones
BRAF V600E
BRAF V600E + anti-IL10RA
WT
WT + anti-IL10RA
d
Mean Extinction Probability
BRAF
BRAF+anti-IL10RA
Extinction Probability
BRAF = 0.54 ± 0.05
BRAF; anti-IL10RA = 0.38 ± 0.05
Days
e
Braf V600E fl/+; IL10RA fl/fl
Tam
Day 0 6 9 14 22
Imaging
f
BRAF IL10RA fl/fl
BRAF IL10RA fl/+
D6
D9
D15
D22
g
Mean % Fixed Clones
BRAF; IL10RA fl/fl
BRAF; IL10RA fl/+
IL10RA fl/fl; k_d^{μ} = 0.59
IL10RA fl/+; k_d^{μ} = 0.44
Days
h
Mean Extinction Probability
BRAF; IL10RA fl/+
BRAF; IL10RA fl/fl
Extinction Probability
IL10RA fl/+ = 0.54 ± 0.048
IL10RA fl/fl = 0.42 ± 0.051
Days
i
BRAF V600E
WT
<0.5
>0.5
IL10RA
TCR/MHC II complex
IL10
Treg

Figure 4. Interleukin 10 receptor (IL10RA) suppresses BRAF^{V600E} selection.

a, Schematic showing experimental design of low-dose, inducible mutagenesis with concurrent, global (antibody mediated) blocking of Il10RA in BRAF V600E*;* VillinCre^{ERT} mice

b, Heat map depicts the relative frequency of clones of the indicated size (columns) in various conditions (rows) for both BRAFV600E and WT clones in the presence of anti-Il10RA or isotype control.

c, Dotplot depicting % of fixed clones for BRAF V600E and WT mice in the presence or absence of Tregs. Each dot represent a mouse with at least 100 clones examined per mice. Error bars represent s.d. of mean.

d, Graph highlights the likelihood of extinction of indicated clone types from the crypt. Shaded areas indicate ± s.d. The extinction probabilities are indicated in the figure (value at 100 days).

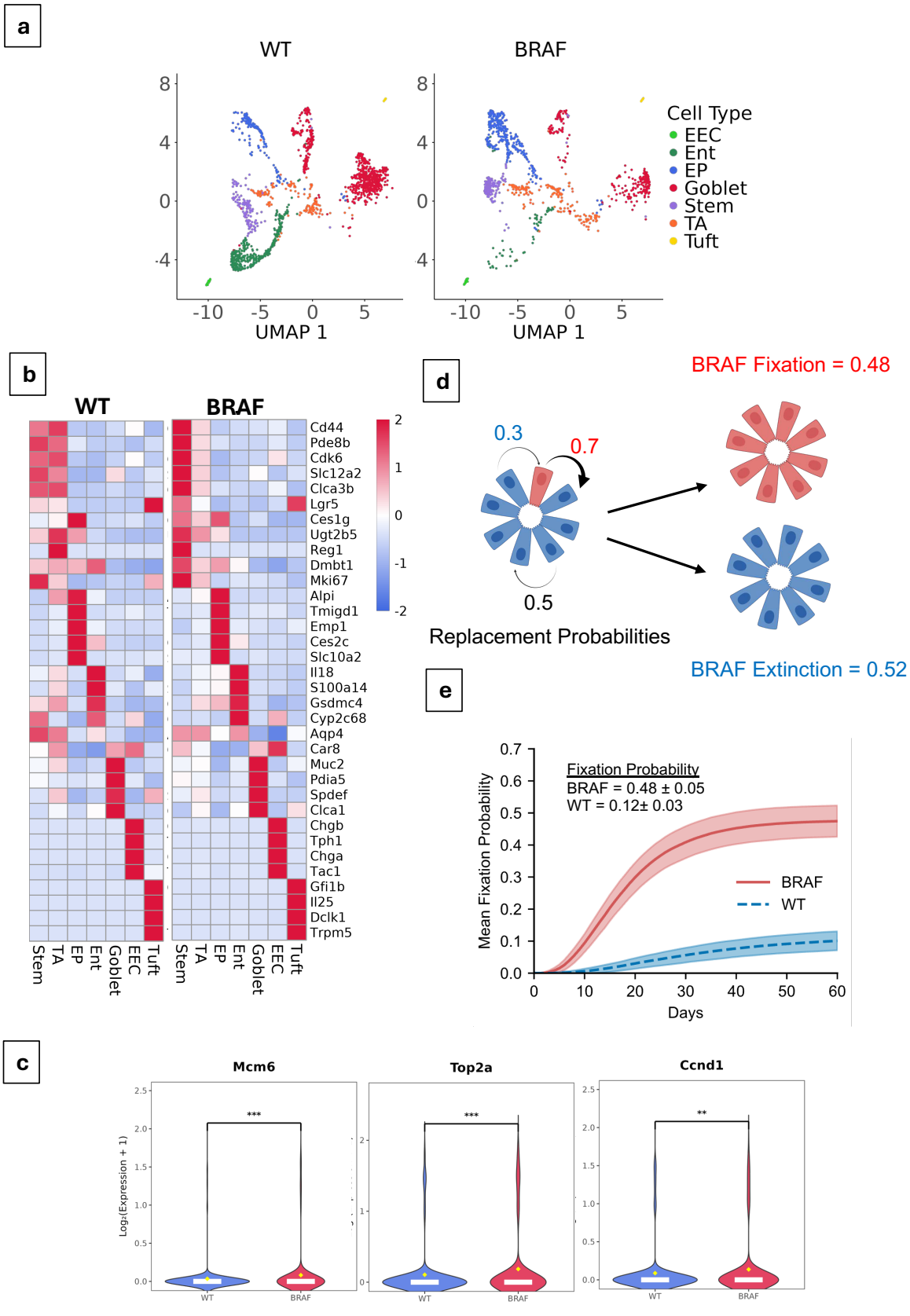
e, Schematic showing experimental design of low-dose, inducible BRAFV600E mutagenesis with concurrent clonal IL10RA deletion.

f, Heat maps depicting the frequencies of clones of the indicated size (columns) at various time points (rows) for both BRAFV600E;IL10RA$^{fl/+}$ and BRAFV600E ;IL10RA$^{fl/fl}$ clones.

g, Probability of % of fixed clones over time as predicted by the SCB model (line ± s.d. as shaded area) and % of fixed clones in experimental data (dots) for BRAF V600E*;*MHCII$^{fl/+}$ and BRAF V600E*;*MHCII$^{fl/fl}$ mice after tamoxifen induction (right). *n* = 5 mice per genotype per time point with at least 100 clones examined per mice. Data (dots) are mean ± s.d. of mean.

h, Graph highlighting the likelihood of extinction of the indicated clone types from a crypt. Shaded areas indicate ± s.d. The extinction probabilities are indicated in the figure (value at 100 days).

i, Cartoon summarizing the mediation of cell-cell competition between BRAF V600E and WT clones by regulatory T cells.


a
WT
BRAF
Cell Type
EEC
Ent
EP
Goblet
Stem
TA
Tuft
UMAP 1
b
WT
BRAF
Cd44
Pde8b
Cdk6
Slc12a2
Clca3b
Lgr5
Ces1g
Ugt2b5
Reg1
Dmbt1
Mki67
Alpi
Tmigd1
Emp1
Ces2c
Slc10a2
Il18
S100a14
Gsdmc4
Cyp2c68
Aqp4
Car8
Muc2
Pdia5
Spdef
Clca1
Chgb
Tph1
Chga
Tac1
Gfi1b
Il25
Dclk1
Trpm5
Stem
TA
EP
Ent
Goblet
EEC
Tuft
d
BRAF Fixation = 0.48
0.3
0.7
0.5
Replacement Probabilities
BRAF Extinction = 0.52
e
Fixation Probability
BRAF = 0.48 ± 0.05
WT = 0.12± 0.03
Mean Fixation Probability
BRAF
WT
Days
c
Mcm6
Top2a
Ccnd1
Log2(Expression + 1)
WT
BRAF

Extended data figure 1: Characterization of epithelial cell types following BRAF V600E mutation leading to clonal fixation.

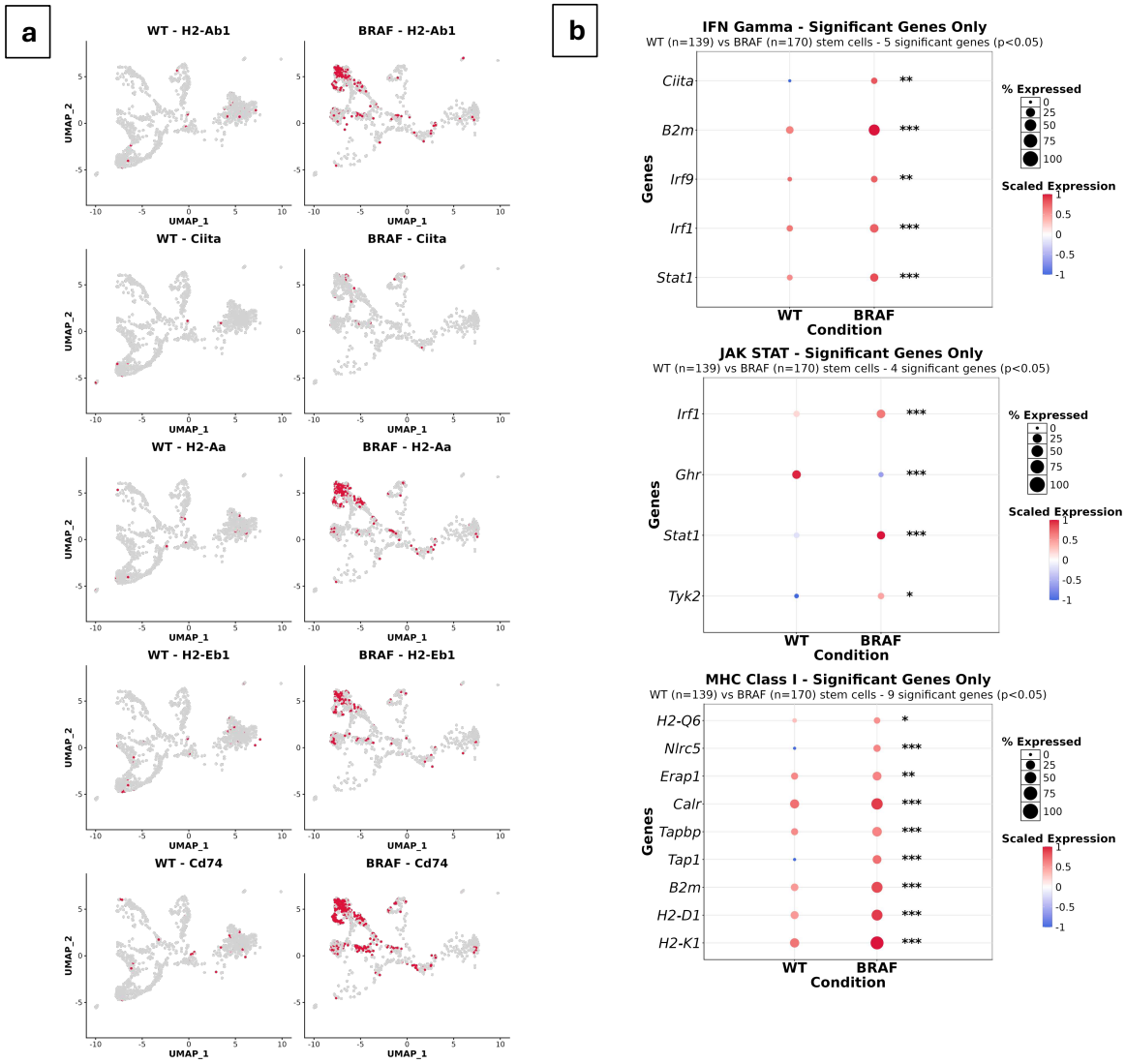
a, Uniform manifold approximation and projection (UMAP) plot showing clustering of epithelial cells based on marker expression: stem cells (Stem), transit-amplifying (TA) cells, enterocyte progenitors (EP), Enterocytes (Ent), enteroendocrine cells (EEC), goblet cells and tuft cells in WT and BRAF V600E mutated mouse colonic epithelium.

b, Heat map representing marker expression for epithelial cells. (Right) groups marker genes for cell types (bottom). Color bar, auto-scaled log_2-transformed normalized UMIs.

c, Violin plot highlighting expression of indicated proliferation markers in the WT and BRAF V600E mutated stem cells, * denotes *p*-value <0.001 (Wilcoxon test).

d, Cartoon depicting the outcome of clonal competition between a single BRAFV600E mutant clone (red) vs WT stem cells in the crypt, leading to crypt fixation or extinction.

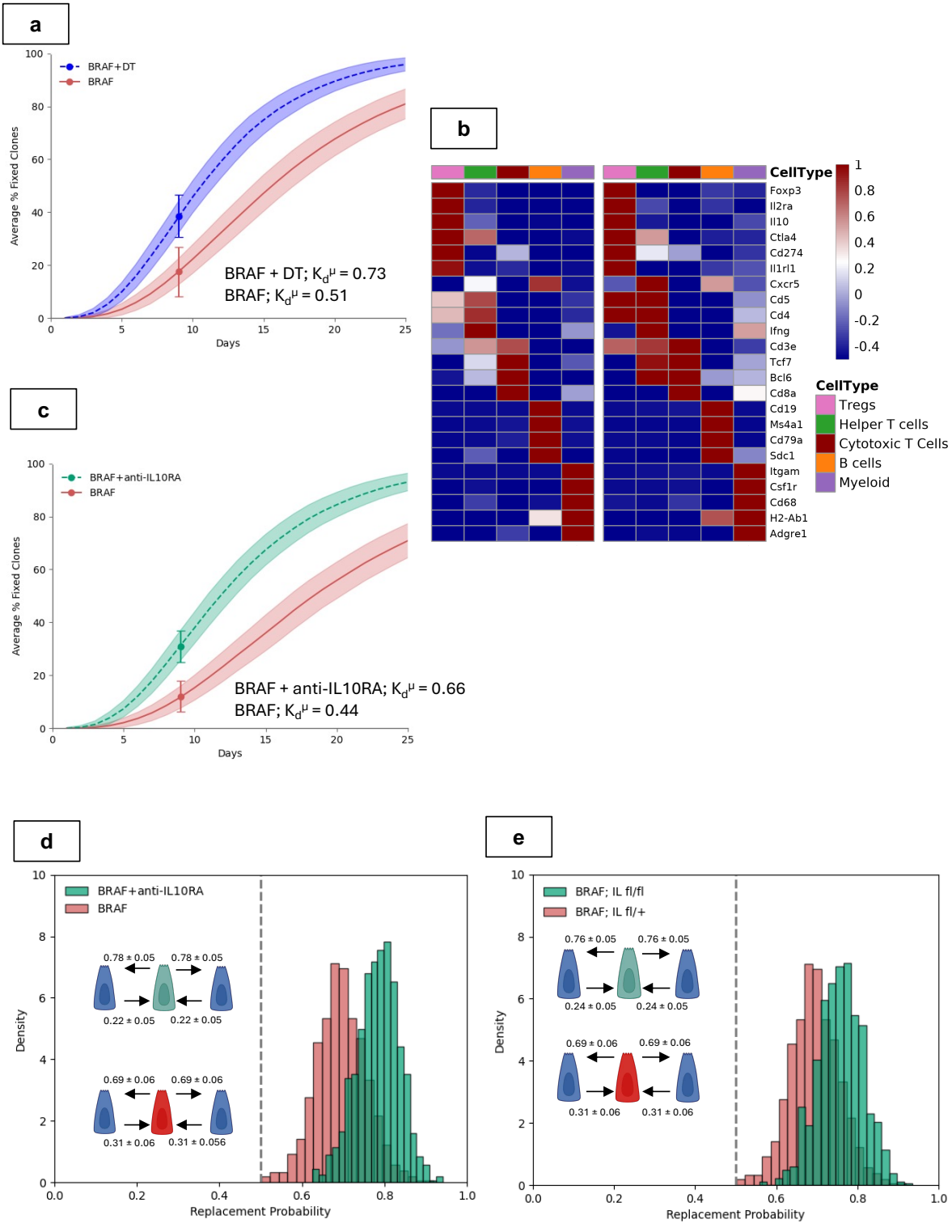
e, Graph depicts the likelihood of the indicated clone types reaching fixation over time. Shaded areas indicate ± s.d. The fixation probabilities are indicated in the figure (value at 100 days).



Extended data figure 2: Characterization of MHCII and related pathway gene expression in epithelial cell types following BRAF V600E mutation leading to clonal fixation.

a, UMAP highlighting increased expression of MHCII pathway genes and their distribution in various cells clusters in WT and $BRAF^{V600E}$ mutated epithelial cells.

b, Dotplots highlighting increased expression of IFNγ (top), JAK-STAT (middle) and MHC class I (bottom) pathway related genes in BRAF V600E mutated stem cells * denotes *p*-value <0.001 (Wilcoxon test).


a
BRAF+DT
BRAF
Average % Fixed Clones
Days
BRAF + DT; K_d^{μ} = 0.73
BRAF; K_d^{μ} = 0.51
b
CellType
Foxp3
Il2ra
Il10
Ctla4
Cd274
Il1rl1
Cxcr5
Cd5
Cd4
Ifng
Cd3e
Tcf7
Bcl6
Cd8a
Cd19
Ms4a1
Cd79a
Sdc1
Itgam
Csf1r
Cd68
H2-Ab1
Adgre1
1
0.8
0.6
0.4
0.2
0
-0.2
-0.4
CellType
Tregs
Helper T cells
Cytotoxic T Cells
B cells
Myeloid
c
BRAF+anti-IL10RA
BRAF
Average % Fixed Clones
Days
BRAF + anti-IL10RA; K_d^{μ} = 0.66
BRAF; K_d^{μ} = 0.44
d
BRAF+anti-IL10RA
BRAF
0.78 ± 0.05
0.78 ± 0.05
0.22 ± 0.05
0.22 ± 0.05
0.69 ± 0.06
0.69 ± 0.06
0.31 ± 0.06
0.31 ± 0.056
Density
Replacement Probability
e
BRAF; IL fl/fl
BRAF; IL fl/+
0.76 ± 0.05
0.76 ± 0.05
0.24 ± 0.05
0.24 ± 0.05
0.69 ± 0.06
0.69 ± 0.06
0.31 ± 0.06
0.31 ± 0.06
Density
Replacement Probability

Extended data figure 3:

a, Probability of % of fixed clones over time as predicted by the SCB model (line with 95% confidence interval shaded area) and % of fixed clones in experimental data (dots) for BRAF V600E in mice treated with diphtheria toxin (DT) after tamoxifen induction (right). *n* = 5 mice per genotype per time point with at least 100 clones examined per mice. Data (dots) are mean ± s.d. of mean.

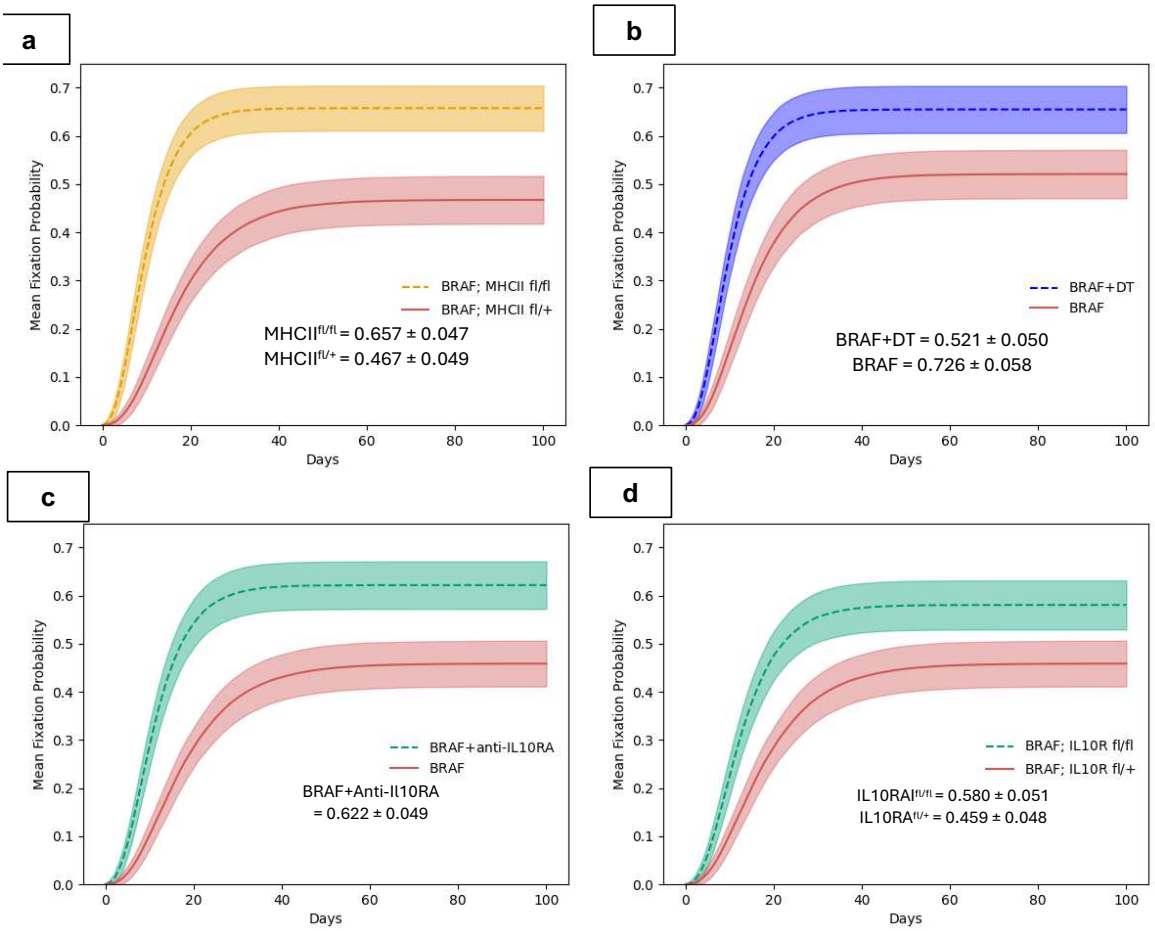
b, Heat map representing marker expression for immune cells (CD45+). (Right) groups marker genes for cell types (bottom). Colour bar, auto-scaled log_2-transformed normalized UMIs.

c, a, Probability of % of fixed clones over time as predicted by the SCB model (line with 95% confidence interval shaded area) and % of fixed clones in experimental data (dots) for BRAF V600E in mice treated with anti-IL10RA after tamoxifen induction (right). *n* = 5 mice per genotype per time point with at least 100 clones examined per mice. Data (dots) are mean ± s.d. of mean.

d, Bayesian inference of the biased drift parameter (replacement probability) for $BRAF^{V600E}$ clones following treatment with anti-Il10RA.

e, Bayesian inference of the biased drift parameter (replacement probability) for BRAFV600E*;* $IL10RA^{fl/+}$ vs $BRAF^{V600E}$*;*$IL10RA^{fl/fl}$ clones.

d and e, The vertical axis indicates probability density. Cartoon summarizes the replacement properties (color coding as in the graphs).



Extended data figure 4: a-d, Graphs depicts the likelihood of the indicated clone types reaching fixation over time. Shaded areas indicate 95% CI. The fixation probabilities are indicated in the figure (value at 100 days).

Supplementary Files

This is a list of supplementary files associated with this preprint. Click to download.

- SupplementaryMaterialBRAFMHCII4.pdf